Journal of Materials Research and Technology 29 (2024) 90–100

Contents lists available at ScienceDirect

Journal of Materials Research and Technology

journal homepage: www.elsevier.com/locate/jmrt

An experimental investigation of the mechanical properties and failure mode of 3D stitched composites

Lucas Moura Montenegro Reis [a], Marcelo Leite Ribeiro [b], Fernando Madureira [b], Arnaldo Carlos Morelli [c], Sergio Neves Monteiro [d,*], Vera Lucia Arantes [a]

[a] Materials Engineering Department, São Carlos School of Engineering, University of São Paulo, 1100, João Dagnone Avenue, Santa Angelina, São Carlos, SP 13563-120, Brazil
[b] Aeronautical Engineering Department, São Carlos School of Engineering, University of São Paulo, 1100, João Dagnone Avenue, Santa Angelina, São Carlos, SP 13563-120, Brazil
[c] Federal Institute of Education, Science, and Technology of São Paulo, Paulo Eduardo de Almeida Prado Municipal Road, Jardim Guanabara, São Carlos, SP 13565-820, Brazil
[d] Materials Engineering Department, Military Institute of Engineering, 80, General Tibúrcio Square, Urca, Rio de Janeiro, RJ 22290-270, Brazil

ARTICLE INFO

Keywords:
Polymer matrix composites. 3D stitched composites. through-the-thickness reinforcement. mechanical properties. failure modes

ABSTRACT

Mechanical behavior and failure modes of three-dimensional (3D) stitched composites were experimentally investigated. In addition, a comparative analysis between these materials and equivalent laminates (2D) was accomplished. The 3D composite plates were manufactured using sheets of glass fiber manually sewn with aramid tows and molded with epoxy resin by vacuum-assisted resin transfer molding. Three-points bending, Charpy impact, double cantilever beam (DCB), and short-beam shear (SBS) mechanical tests were carried out on both types of materials. The DCB test results revealed that the action of reinforcement tows inhibited the propagation of the delamination cracks, which led to an increase in the fracture toughness of the 3D composites. However, the damage caused by the stitching process, such as fiber breakage and misalignment as well as crimping, and resin-rich regions, was responsible for reducing the flexural and shear properties of these materials. In addition, it was revealed that the stitching did not influence the impact toughness, although it prevented delamination from quick propagation, avoiding a catastrophic failure, which enhanced the damage tolerance of these materials, mainly for aeronautical applications.

1. Introduction

Three-dimensional (3D) composites were developed to mitigate the weaknesses presented by traditional two-dimensional (2D) laminates, such as low interlaminar fracture toughness ($G_{Ic} < 150$ J/m^2) and high susceptibility to delamination. The manufacturing of 3D composites can be achieved through various techniques, including weaving, braiding, knitting, Z-pinning, and stitching [1–5]. The stitching method, originally developed for joining composite material structures, involves the insertion of reinforcing tows (usually made of carbon, glass, or Kevlar fibers) in the thickness direction using sewing machines. This technique has demonstrated its capability to enhance interlaminar properties and damage tolerance, rendering 3D stitched composites highly promising for applications across diverse industrial sectors, such as aeronautics, aerospace, automotive, and military defense equipment [6–10].

Numerous studies were conducted to assess the mechanical properties of 3D composites, investigating stitching parameters and patterns. In a study by Zhao et al. [11], a significant 44 % increase in Charpy impact resistance was observed in 3D composites compared to 2D laminates. The increase was attributed to enhancing the ductility of these composites through stitching. Similar findings were reported by He et al. [6], using drop-weight testing to evaluate the impact properties of stitched composites, varying stitching patterns and densities. The study highlighted the capacity of stitching to inhibit delamination and reduce out-of-plane deformation, resulting in an increase in low-speed impact resistance.

In contrast, Ravandi et al. [12] found, through drop-weight tests, that stitching had a negative impact on the strength of 3D composites. The authors argued that resin-rich regions generated during the reinforcement process had lower crack propagation resistance, leading to a

* Corresponding author.
E-mail address: sergio.neves@ime.eb.br (S.N. Monteiro).

https://doi.org/10.1016/j.jmrt.2023.12.283
Received 1 November 2023; Received in revised form 26 December 2023; Accepted 31 December 2023
Available online 14 January 2024

reduction in the required load for damage initiation.

Regarding the behavior under flexural loads, Kaya et al. [13] observed a significant reduction of up to 26 % in flexural strength due to the presence of stitches. This decrease was attributed to damage introduced during the reinforcement process, such as resin-rich regions, breakage and misalignment in the in-plane fibers. However, in contrast, the authors noted a substantial increase in flexural toughness. This increase was associated with the ability of the reinforcement tows to improve deformation energy absorption, resulting in an enhancement of damage tolerance for these materials. These results are consistent with the findings of Mouritz [14] and Mouritz et al. [15], but they contrast with the findings of Nie et al. [16], who reported no influence of stitching on flexural strength for low stitch densities and a reduction as stitch density increases.

Fracture toughness is a property often enhanced by the stitching process. A notable example is demonstrated in the comparative study by Velmurugan and Solaimurugan [17], which found that stitching significantly inhibits delamination crack propagation through the application of compressive force. This mechanism reduces the tensile force at the crack tip, resulting in a remarkable increase of up to 20 times in interlaminar fracture toughness in mode I. These results align with findings from other studies, such as those conducted by Dransfield et al. [18] and Mouritz [15]. Additionally, work conducted by Plain and Tong [19] revealed that reinforcement tows with larger diameters can increase interlaminar fracture toughness by up to 100 % in the early stages of crack propagation. However, as the crack advances, efficiency decreases as stitching bridges can no longer suppress the crack.

In the study by He et al. [20], the analysis of shear strength in short-beams revealed a complex influence of stitching. They found that the presence of stitches reduces the elastic limit of the 3D composite due to the presence of resin-rich regions. However, simultaneously, stitching increases damage tolerance. A crucial aspect highlighted by the authors was the importance of the distance between reinforced regions and applied load. It was observed that large distances between stitch points mitigate the negative effect of resin-rich regions since the stitch points are not located within the loaded region. These results align with the findings of Mitschang and Ogale [21] but are in contrast with the results found by Jain and Mai [22], who reported no influence of stitching on shear strength.

The challenge in implementing stitched 3D composites as structural materials stems from conflicting data regarding the extent of improvement and deterioration that stitching might cause [23]. This discrepancy can be elucidated by analyzing the failure mode of 3D stitched composites, which involves a “competition” between the advantages brought by reinforcement, such as enhanced damage tolerance and interlaminar fracture toughness, and the disadvantages, including damage incurred during the stitching process, as well as breakage and misalignment in the in-plane fibers, including the formation of resin-rich regions, and fiber crimping [24–27]. Furthermore, several authors [14, 28–30] correlate the amount of damage introduced during the reinforcement process with stitching parameters, such as stitch density, reinforcement tow diameter, stitch types, and stitching pattern.

In this work, layers of fiberglass were manually stitched with aramid (Kevlar) tows, forming a 3D architecture known as a plain stitch. A high stitching density and a large diameter of reinforcement tows were employed to achieve the maximum crack propagation resistance possible. Subsequently, the preforms were impregnated with epoxy resin using the vacuum-assisted resin transfer molding method (VARTM). Three-point bending, double cantilever beam, Charpy impact, and short-beam interlaminar shear tests were conducted on both stitched 3D composite samples and 2D laminates to generate comparative data. These tests aimed to contribute to the technological maturity of these materials by establishing a definitive answer regarding the influence of stitching on laminate properties. Finally, optical microscopy was employed to analyze composite samples, identifying the mechanisms that caused failures in these materials.

2. Materials and methods

2.1. Materials

The composites were manufactured from fourteen layers of bi-directional glass plain weave fabrics (model WR-326, consisting of E-type glass fibers with a grammage of 326 g/cm^2). To fabricate the preforms, sheets of glass fiber were stitched with Kevlar tows of the K-336 model (tex 336). These Kevlar tows have a tensile strength of 2950 MPa and a low density of 1.44 g/cm^3. This combination of properties, along with high impact resistance, makes the Kevlar tow an ideal material to be utilized as a sewing thread [17].

The system used to impregnate the composites consisted of an RLL EX 10607 model resin and the HALL 115 catalyst. This resin was specially developed for composite molding processes, including laminations and impregnation, due to its low viscosity that enhances fiber wetting. The viscosity and density values of the resin at 25 °C are 550 mPa s and 1.15 g/cm^3, respectively.

2.2. Manufacturing

To manufacture the preforms, glass fiber layers were stacked on top of each other in a sequence of 0°/90° and then affixed to a Styrofoam plate, with a template inserted over the fibers. This template serves as a guide for the stitching procedure and features a grid where the height of the squares represents the pitch and base spacing. The stitching process involves inserting a needle with a Kevlar tow at one vertex of the square, guiding the needle to emerge from the opposite side of the mold at the same vertex while passing through all the sheets of glass fiber. Fig. 1 illustrates schematically the stitching process carried out, also highlighting the stitching pattern used for all samples.

The Kevlar tows were stitched parallelly to the length of the samples, forming a plain stitch architecture. The same stitch parameters were used for all 3D specimens, consisting of a pitch and spacing of 6 and 4.5 mm, respectively, generating a density of 0.037 mm^{-2}, as calculated using the following equation:

$$SD = \frac{1}{s.p} \tag{1}$$

where SD is the stitch density, s is the spacing, and p is the stitch pitch.

The laminated was impregnated with epoxy resin using VARTM. The curing process took place at room temperature (RT) for 24 h. In total, six composite plates were manufactured, consisting of three plates of each configuration, 3D and 2D, cut to the dimensions of the samples related to the test to be carried out.

2.3. Experimental procedure

As part of the experimental process, four types of mechanical tests were conducted: (i) Three-points bending; (ii) Charpy impact; (iii) DCB; and (iv) SBS. In addition, the density (ρ), fiber volumetric fraction (V_f), matrix volumetric fraction (V_m), and thickness (t) of both the 3D and 2D samples were evaluated to facilitate a comprehensive comparison between the two composite configurations. Sample specifications for each test are presented in Table 1.

The influence of fiber volumetric fraction on the mechanical behavior of composite materials is evident, with higher fractions often correlating with superior performance due to the load-bearing capacity of the fibers. However, in the (VARTM) infusion technique utilized for molding in this work, achieving identical infusion parameters proves challenging, leading to variations in fiber volumetric fractions among samples. Therefore, it is crucial for these values to be closely aligned to facilitate valid comparisons.

The slight difference in V_r (with the largest being 2 % in samples subjected to the DCB test) suggests that this parameter has a significantly

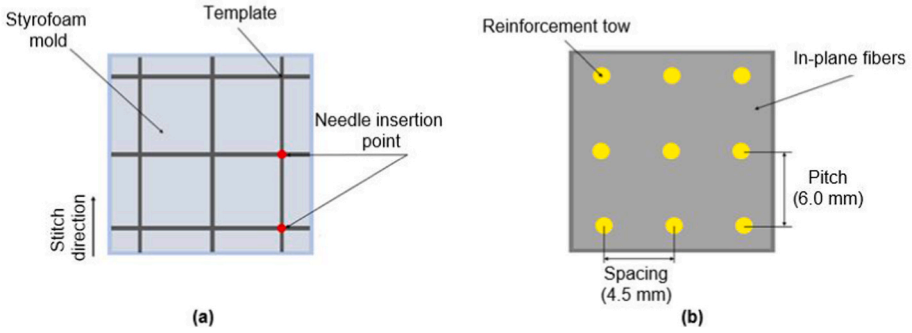

Fig. 1. Schematic of (a) completely stitch closed mold and (b) stitch pattern in the dry preform.

Table 1
Specimens' specifications according to the test.

Tests	ρ (g/cm^3)	t (mm)	V_r (%)	V_m (%)
Three-points bending				
3D	1.89 (±0.11)	3.70 (±0.07)	56.76 (±0.27)	40.01 (±0.62)
2D	1.97 (±0.10)	3.49 (±0.05)	57.23 (±0.29)	38.94 (±0.66)
Charpy impact				
3D	1.84 (±0.04)	3.73 (±0.08)	50.49 (±0.07)	47.57 (±0.16)
2D	1.89 (±0.02)	3.17 (±0.40)	51.67 (±0.22)	44.84 (±0.51)
Double-cantilever beam				
3D	1.80 (±0.04)	3.71 (±0.18)	48.39 (±0.05)	44.58 (±0.13)
2D	1.83 (±0.03)	3.69 (±0.03)	49.59 (±0.25)	41.81 (±0.59)
Short-beam shear				
3D	1.89 (±0.11)	3.65 (±0.03)	56.76 (±0.27)	40.01 (±0.62)
2D	1.97 (±0.10)	3.30 (±0.37)	57.23 (±0.29)	38.94 (±0.66)

smaller impact on the evaluated properties compared to the stitching process.

2.3.1. Three-points bending test

Three-points bending tests were conducted at RT according to ASTM D7264 [31]. For statistical purposes, seven samples of each configuration were manufactured. The distance between the fixed supports was 111.68 mm and 118.40 mm for 2D and 3D specimens, respectively. The strain rate used was 1 mm/min. As in composites molded by the VARTM technique, there is a difference in surface roughness between the upper and lower surfaces. Therefore, all specimens were tested with the rough surface in contact with the load support.

The flexural stress and strain were calculated using Eq. (2) and (3), respectively. In these equations, P represents the load, L denotes the span, b stands for the width, t represents the thickness, and D corresponds to the deflection. The flexural elastic modulus was determined based on the slope of the line in the elastic region.

$$\sigma_f = \frac{3PL}{2bt^3} \tag{2}$$

$$\varepsilon = \frac{6Dt}{L^2} \tag{3}$$

2.3.2. Charpy test

Charpy impact tests were performed to assess the impact resistance of the composite materials in accordance with ASTM D611 [32]. While the standard stipulates that the samples should ideally have a maximum length of 127 mm, a thickness of 3–12.70 mm, and a width equal to the thickness—provided the thickness value falls between 3 mm and 12.70 mm—adjustments to the specimen dimensions were necessary to accommodate the predetermined stitch density for the sewing procedure. Thus, seven specimens of each composite configuration were manufactured, each having a length of 127 mm, width of 12.70 mm, and thickness of 3.70 mm.

Subsequently, the samples were notched using equipment suitable for this type of machining. The notch depth was set at 2 mm, and the angle was maintained at 45°, as per the standard's recommendations [26].

2.3.3. Double cantilever beam test (DCB)

To assess the resistance of the composite material to delamination cracks, mode I interlaminar fracture toughness tests were conducted, following the recommendations outlined in ASTM D5528 [33]. For this purpose, three specimens of each configuration were prepared, each featuring a length of 125 mm, a width of 23 mm, and a thickness of 3.70 mm. To introduce an initial crack of 60 mm length, a non-adhesive film of polytetrafluoroethylene (Teflon®) was inserted into the mid-plane of the specimens. It is important to note that the section containing this non-adhesive film was left unstitched. Hinges were initially affixed to the samples using cyanoacrylate superglue. However, due to the insufficient adhesion between the glue and the specimens, especially under high loads in the case of 3D composites, a more robust arrangement involving M6 bolts was devised to facilitate proper test execution. Although cyanoacrylate glue sufficed for testing 2D composite samples, all specimens were ultimately outfitted with M6 bolts to maintain test standardization.

The laminate fracture toughness (G_{Ic}) was evaluated using the Irwin-Kies equation, with compliance reduction method (C) based on the principles of the Simple Beam Theory (SBT) [27].

Irwin Kies equation:

$$G_{Ic} = \frac{P^2}{2b}\frac{dC}{dA} \tag{4}$$

Simple Beam Theory (SBT):

$$C = \frac{2}{3}\frac{a^3}{E_f I} \tag{5}$$

Here, the symbol C represents the compliance (δ/P), where δ denotes displacement, P means the load, a corresponds to the delamination length, b indicates the width of the sample, E_f represents the bending elastic modulus, and I denotes the second moment of inertia of the sample. The latter is calculated by Eq. (6), with t representing the thickness.

$$I = \frac{bt^3}{12} \tag{6}$$

Since compliance can be experimentally determined through tests, the crack length can be back-calculated from Eq. (7) using the equivalent crack approach:

$$a = \left(3 \,.\, C \,.\, E_f \,.\, \frac{I}{2}\right)^{1/3} \tag{7}$$

2.3.4. Short-beam shear test (SBS)

To conduct the shear strength test, the ASTM D2344 [34] standard was employed as a reference. Four samples of each composite

configuration were manufactured for this purpose. The strain rate applied during the test was set at 1 mm/min. Furthermore, the loading noses and supports utilized had diameters of 3 mm and 1.50 mm, respectively, adhering to the specifications of the standard. Similar to the procedure in the three-points bending test, all specimens were tested at RT, with the rough surface of the specimen in contact with the crosshead. It is worth noting that, in this test, the span was defined at a 4:1 ratio to the thickness of the samples, measuring 14.6 mm for 3D composites and 13.2 mm for 2D laminates. This standardized approach ensured consistent testing conditions and accurate comparative results.

The test was concluded after recording a 30 % load drop and a load curve. In this type of test, there is no need to construct a stress versus displacement graph, as the calculation of interlaminar shear strength is determined by the maximum force values, as shown in Eq. (8).

$$\tau = 0,75\frac{P_{max}}{bt} \tag{8}$$

3. Results and discussions

3.1. Defects caused by the stitching process

Fig. 2 illustrates fiber misalignment, a prevalent damage observed in all 3D composite specimens. This defect emerges from the spreading of fibers within the plane due to the stitching process, consequently inducing localized tension in the affected area. Furthermore, this misalignment detrimentally affects the adhesion between the reinforcement tow and the surrounding matrix, ultimately leading to a reduction in the mechanical performance of 3D composites, particularly under bending loads and interlaminar shear stresses.

By contrast, significant levels of fiber breakage surrounding the reinforcement tow were not detected. The mitigation of this particular defect can be attributed to the manual sewing technique and the utilization of the plain stitch architecture in this study. It is worth noting that stitching conducted by automated machines often results in extensive fiber misalignment, breakage, and crimping within the plane, owing to the high sewing tensions these machines employ [14].

Another prevalent defect observed is reinforcement tow distortion, as depicted in Fig. 3. This phenomenon arises from the compaction of the preform during the molding process, which subsequently impacts the strain energy absorption capacity of the reinforcement when subjected to a load. Specifically, the stitch becomes compressed as the fibers compact due to vacuum bagging. This results in a stress distribution that is more conducive to failure within the reinforcement tow, thereby compromising its structural integrity and hindering its ability to deform as expected under applied loads.

Fig. 4 illustrates infusion defects located on the surface of the preforms around the reinforcement tows. These defects can be associated with crimping, which is caused by angling and distorting fibers in the plane during the stitching process. The crimping process has a critical influence on the failure mechanism of 3D composites, as it creates surface defects, which act as stress concentrators and subsequently induce deeper cracks in the matrix, resulting in a reduction in the mechanical properties of these materials.

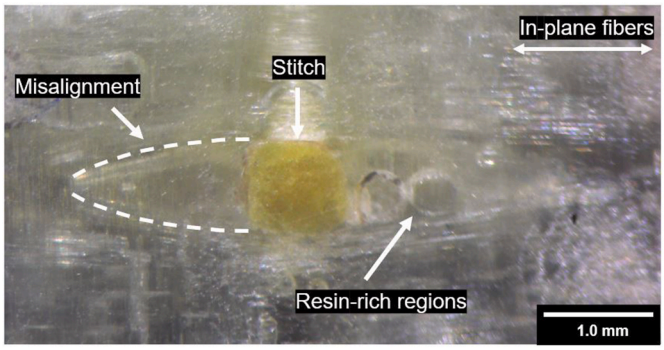

Fig. 2. Misalignment caused by the reinforcement tow in 3D composites.

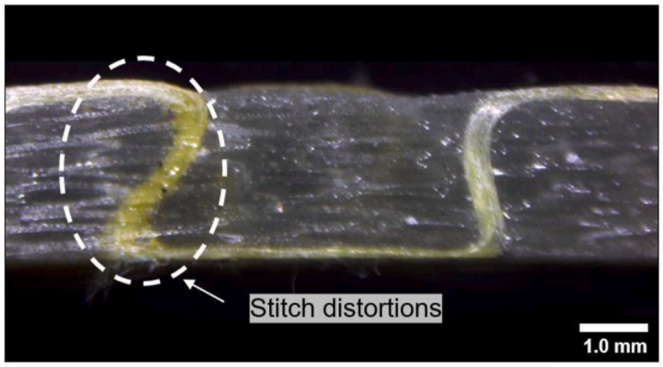

Fig. 3. Stitch distortions.

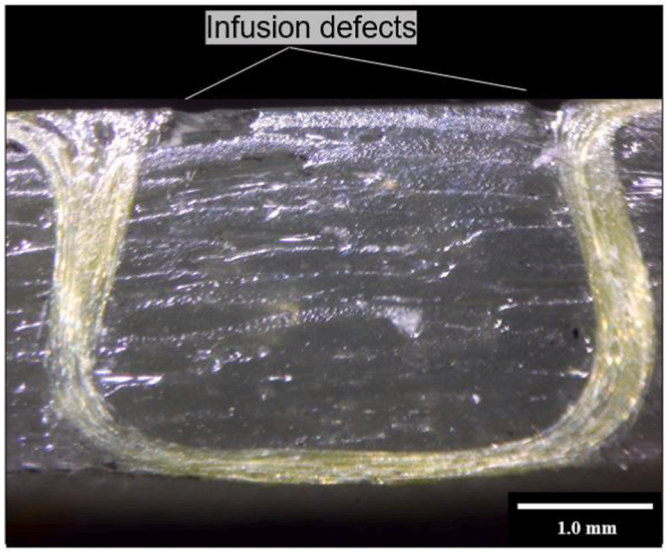

Fig. 4. Infusion defects caused by crimping around the reinforcement tows.

It should be noted that the stitch defects described in this topic have been observed, to a greater or lesser extent, in all 3D composite specimens. It is possible to state that the amount of such defects depends on how the stitching and infusion process is carried out.

3.2. Flexural properties

Fig. 5 presents the characteristic load-deflection curves of both 3D and 2D composites under the three-points bending test. Notably, a discernible non-linearity is evident in the final phase of the curve pertaining to the 3D composites, in stark contrast to the 2D laminates that exhibit a precipitous drop shortly after reaching complete failure. This nonlinearity arises due to the formation of a stitch bridging zone. The formation process is as follows. First, delamination occurs, prompting the initiation of a stitch bridging phenomenon that initially curtails the progression of the delamination crack. Second, with a progressive escalation in the bending load, the delamination advances, causing the breakage of the first reinforcement tow and subsequently moving on to the next tow, which experiences a similar event. This cycle culminates in ultimate failure. Notably, each instance of delamination breaking a sewing thread and moving to the next, results in a punctual increase in the load, a mechanism depicted in Fig. 6.

By contrast, 2D composites exhibit an abrupt load drop, indicative of

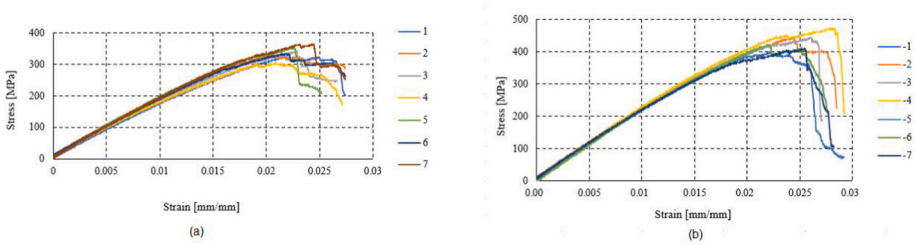

Fig. 5. Typical stress-strain curve of (a) 3D and (b) 2D composites in the three-points bending test.

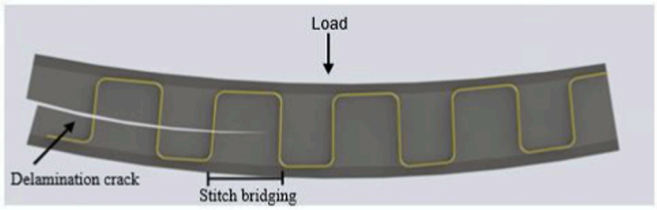

Fig. 6. Schematic drawing of delamination crack propagation in 3D stitched composites subjected to three-points bending test.

catastrophic delamination crack propagation. Despite their comparatively lower resistance to bending loads, 3D composites retain their structural integrity, even post-failure, enhancing the overall damage tolerance of these materials. This ability to withstand failures and facilitate intermittent repairs can significantly contribute to prevent structural accidents [28,35]. Furthermore, it is worth highlighting that 2D laminated composites demonstrate higher tenacity compared to their 3D counterparts, indicating that the reinforcement tow does not contribute as significantly to energy absorption as anticipated.

Table 2 provides a comprehensive overview of the key values acquired from the three-points bending test. Notably, 3D composites exhibit a 22 % reduction in flexural strength and a 19 % reduction in stiffness when compared to their 2D laminate equivalents. This reduction is primarily attributed to damage incurred during the stitching process, including fiber breakage, misalignment, and the presence of resin-rich areas (Fig. 7). Fiber breakage in the vicinity of stitching points fails to support compressive stresses on the upper part of the specimens, thereby overloading adjacent fibers. Additionally, the formation of kinking bands on the material's surface is prone to occur in regions of significant misalignment and crimping. These combined mechanisms contribute to premature failures in 3D composites, consequently translating to diminished strength and flexural elastic modulus. The nearly 20 % decrease in flexural properties caused by defects stemming from the stitching process was corroborated by other researchers [13,14,36–38].

In contrast to the behavior observed in 2D composites, delamination cracks in 3D composites were not detected in close proximity to kinking band regions, as visually demonstrated in Fig. 8. This notable disparity can primarily be attributed to the reinforcing effect of the tows within the 3D composite structure, effectively retarding the propagation of delamination cracks. Consequently, it is reasonable to infer that the stitching process contributes to an enhanced damage tolerance in 3D composites.

This distinctive response underscores the potential of 3D composites

Table 2
Mechanical properties obtained in the three-points bending test.

Specimens	Flexural strength [MPa]	Flexural elastic modulus [GPa]	Maximum ductility [mm/mm]
3D	334.09 (±19.20)	16.13 (±0.89)	0.027 (±0.001)
2D	432.83 (±24.83)	20.10 (±0.69)	0.027 (±0.001)

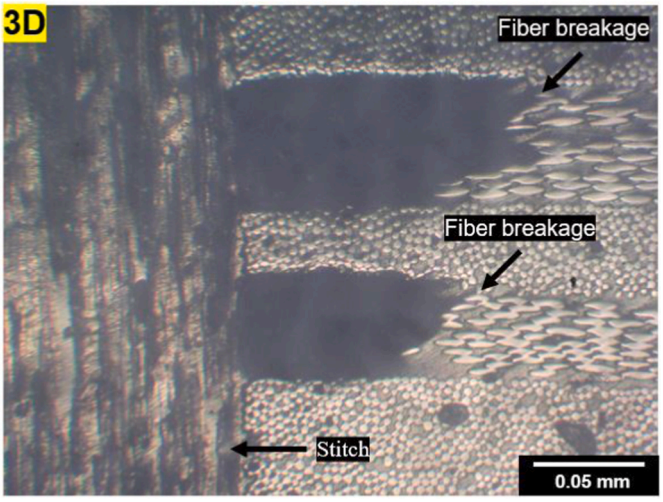

Fig. 7. Damage caused due to the stitching process.

to mitigate and suppress delamination-related failure mechanisms, thanks to the intrinsic capability of the reinforcement tows to impede crack propagation. This is a noteworthy advantage that distinguishes 3D composites from their 2D counterparts.

It is important to highlight that elevated stitching density and increased reinforcement tow diameter have exacerbated the detrimental effects induced by the stitching process. This has culminated in a more pronounced reduction in both the flexural strength and flexural elastic modulus of the 3D composites. These findings underscore the critical role that stitching parameters play in influencing the structural integrity and mechanical properties of 3D composites. The intricate interplay between stitching density, reinforcement tow diameter, and resultant damage emphasizes the need for precise process control to optimize the performance of these composite materials.

Moreover, the findings in this work align with existing literature, indicating a general tendency for flexural properties to deteriorate with the stitching process. While studies, such as Nie et al. [16], have reported a slight increase linked to the stitching's ability to inhibit delamination. It is commonplace to observe that damages caused by stitching, including resin-rich regions, in-plane fiber breakage and misalignment exert a significant impact, leading to a decrease in strength. This observation is in line not only with the results of this study but also with the findings of Mouritz [14], Mouritz et al. [15], and Kaya et al. [13]. An effective strategy to enhance flexural strength seems to be the use of smaller stitching parameters and smaller tow diameters.

3.3. Impact toughness

Similar failure mechanisms were observed in 2D and 3D composites subjected to low-impact loads, encompassing matrix cracks, fiber breakage (see Fig. 9), and delamination. Among these mechanisms, the delamination crack emerges as the predominant cause of structural

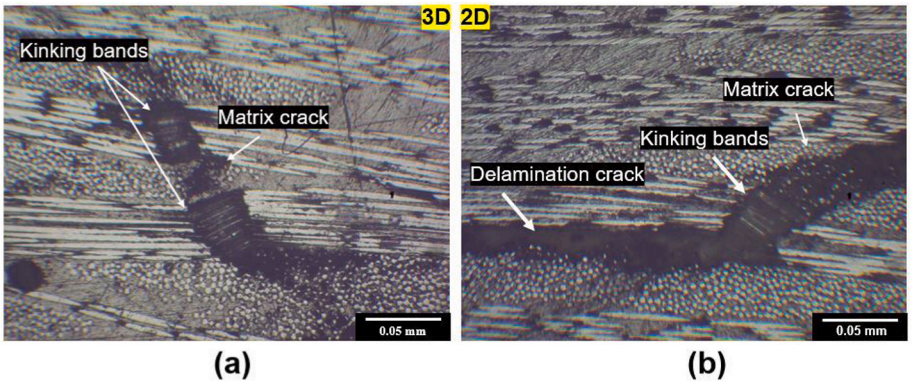

Fig. 8. Kinking band regions in (a) 3D and (b) 2D composites.

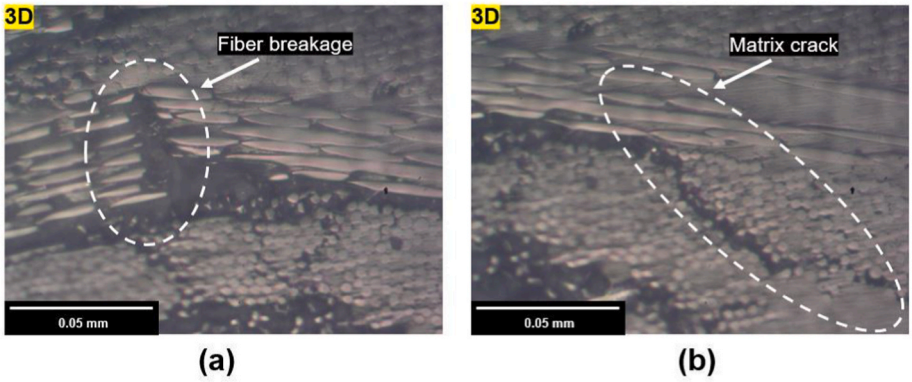

Fig. 9. (A) In-plane broken fibers and (b) Cracks in the matrix.

failure in both composite configurations, leading to a consequential stiffness reduction. Notably, a comparative analysis reveals a distinct behavior. In 2D laminate composites, a single delamination event occurs, whereas in their 3D counterparts, multiple short delamination cracks form in proximity to the impact zone, as depicted in Fig. 10. This distinction arises due to the inherent dissimilarity between the two configurations. In the 2D composites, the absence of crack-inhibiting mechanisms facilitates linear crack propagation until ultimate failure. Conversely, the intricate architecture of 3D composites initially restrains crack propagation through the reinforcing tows. Subsequently, the appearance of discrete microcracks mitigates the propagation velocity of the primary delamination fracture, introducing a multi-stage cracking process.

Table 3 outlines the impact toughness values and the maximum observed crack lengths for both composite configurations. Notably, no statistically significant difference was observed in the absorbed impact energy between the two configurations, defying initial expectations. Despite the inherent capability of 3D composites to curtail delamination crack propagation velocity, suggesting heightened impact resistance compared to their 2D counterparts, the experimental data intriguingly contradicts this hypothesis. This surprising result is attributed to the

Table 3
Impact toughness values.

Specimens	Impact energy [kJ/m^2]	Maximum length of delamination [mm]
3D	222.74 (±23.49)	7.09
2D	237.17 (±24.56)	12.00

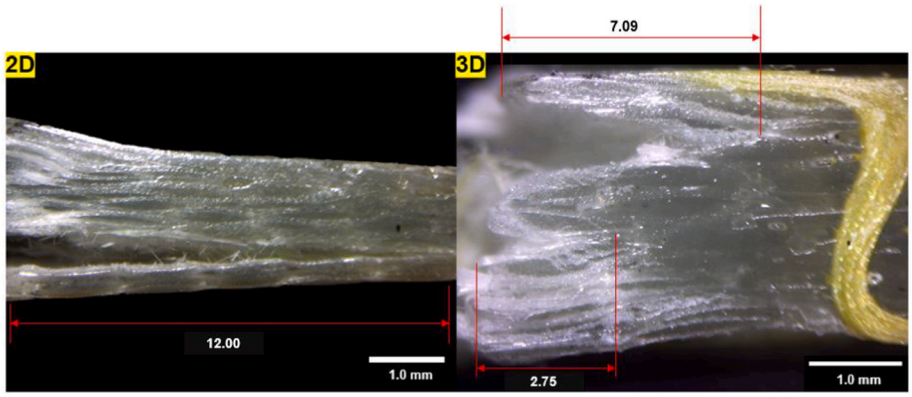

Fig. 10. Comparison between the length of delamination cracks in 2D and 3D composites.

intricate interplay of factors, particularly the influence of the stitching mechanism.

The impact of stitching on impact toughness can be ascribed to the morphology of the delamination cracks. The intrinsic action of reinforcing tows prevents the propagation of the crack across the entire specimen, leading to the formation of limited-length delaminations. These diminutive cracks exhibit insufficient extent to enable the full maturation of stitch bridging zones, consequently rendering the stitching mechanism ineffectual in substantially suppressing these short cracks (see Fig. 11). Notably, since the length of such delaminations remains below the maximum length attained by delaminations in the 2D composites, this phenomenon is revealed as an advantageous outcome caused by the stitching mechanism. It serves to avert catastrophic and abrupt failures induced by rapid large-delamination crack propagation.

Moreover, the absence of a significant impact on absorbed energy due to the presence of stitching can be attributed to the intricate interplay between the benefits and drawbacks introduced by the reinforcement process. While the reinforcement effectively restrains excessive growth of delamination cracks, it simultaneously introduces certain defects, such as fiber breakage and misalignment, which contribute to a decline in the 3D stitched impact resistance.

Notably, the contrast between stitching's impact on low-energy impact strength and its pronounced effects on other mechanical properties, particularly the notable deterioration observed in flexural strength and interlaminar shear strength, is intriguing. This discrepancy suggests that optimizing impact resistance through stitching requires precise parameter adjustments. The determination of optimal stitching parameters is considered to depend on the in-plane fiber architecture and grammage, and the material of these layers. In studies where an increase in impact resistance was observed, such as in the works of Zhao et al. [11] and He et al. [6], this increase is generally attributed to the fact that the damages caused by the stitching process, such as the creation of resin-rich regions, fiber breakage, misalignment in the plane, and crimping, had less impact than the benefits, such as the suppression of post-impact crack delaminations and the increased energy absorption capacity generated by the reinforcement tow.

Different from these results, the study conducted by Ravandi et al. [12] indicated that damages had a more significant impact on the performance of 3D composites, resulting in a reduction in this property. In summary, the discrepancy in the performance of 3D composites observed in previous studies seems to be intrinsically linked to the specific stitching parameters used.

Unfortunately, there is a scarcity of works that quantify the benefits generated in relation to the damages resulting from the insertion of the reinforcement tow. This topic remains a wide field to be explored, providing the opportunity to evaluate which stitching parameters are ideal according to project requirements.

3.4. Mode I interlaminar fracture toughness

One of the primary advantages predicted by the implementation of stitching is a significant increase in interlaminar fracture toughness. Comparative analyses between 2D and 3D composites have consistently demonstrated that reinforcement tows can strongly suppress the propagation of delamination cracks [17,18,39,40]. The effect of increased fracture toughness in the 3D specimens studied in this work is illustrated in Fig. 12. Notably, in both composites, the load increases linearly until the onset of crack propagation. At this juncture, the initial load is comparable in both 3D and 2D composites. However, as the displacement gap widens, the load required to propagate delamination in the 3D composite increases at a higher rate.

Upon reaching maximum load, both materials exhibit a sudden decay in stress values. However, the behavior of 2D and 3D composites diverges. While 2D composites stabilize at a relatively consistent stress level until complete failure, the 3D composites exhibit a unique behavior. Close to a displacement of 20 mm, the 3D composites register a transient increase in load, similar to what was observed in the Three-points bending test. This phenomenon is a result of the action of the reinforcement tows. Initially, as the first sewing thread carries the load, it serves as the sole active reinforcement tow. Subsequently, minimal propagation of the delamination crack occurs without breaking the first thread, creating what is known as the stitch bridging zone. At this stage, the second tow becomes engaged, leading to renewed stress accumulation (Fig. 13). This process continues until the arm of the 3D composite specimens fails due to bending, making it impossible to calculate G_{Ic}. A similar bending-related failure in 3D composite samples during the DCB test was documented by other authors, who proposed modifications to the DCB sample geometry and testing methodology [19,41].

The exceptional resistance of 3D composites to delamination crack propagation, as observed in this study, can be exclusively attributed to the 'stitch bridging' mechanism [13]. This mechanism exerts compressive forces that effectively reduce the tensile stress acting on the crack tip. Additionally, the high values of stitching density and diameter of the reinforcement tow are likely to contribute to the near-complete inhibition of delamination crack propagation, necessitating alternative failure mechanisms.

Summarizing the data obtained from the DCB test, Table 4 underscores the superiority of 3D specimens, presenting a maximum load 66 % higher than their 2D counterparts. This observation aligns with expectations, given the restraining effect of the reinforcing tows on the catastrophic propagation of delamination cracks. Notably, the maximum displacement in 3D composites is also greater. However, it is important to acknowledge that part of this displacement and stress in the 3D samples, as indicated in Table 4 and Fig. 10, corresponds to the bending of specimen arms. This displacement occurs due to minimal delamination propagation and ceases once the initial loads are applied. Consequently, while quantitative data provides valuable insights, conclusions drawn from this test are predominantly qualitative.

Considering the failure mode analysis of 3D composites, it is plausible that the 'stitch bridging' mechanism efficiently inhibits delamination crack propagation – a critical failure mode in fiber polymer reinforced (FPR) composites. The efficacy is evident even in the DCB test, where the applied load primarily induces opening. The fact that the samples failed due to other mechanisms, such as bending of the upper arm, matrix cracks, and surface fiber ruptures, suggests that the 'stitch bridging' mechanism was remarkably effective.

Additionally, examining Table 4, a significant 98.43 % reduction in delamination crack length is evident in 2D composites compared to their

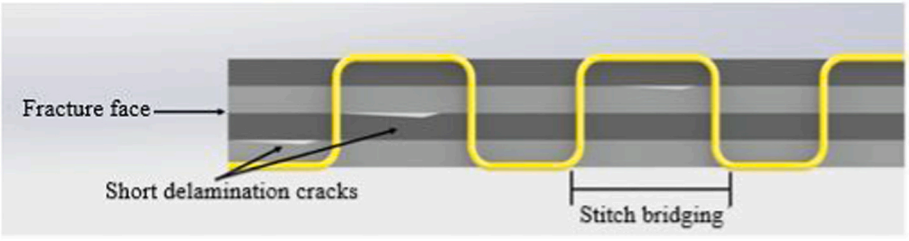

Fig. 11. Schematic drawing of short delamination cracks that are not inhibited by the stitch bridging.

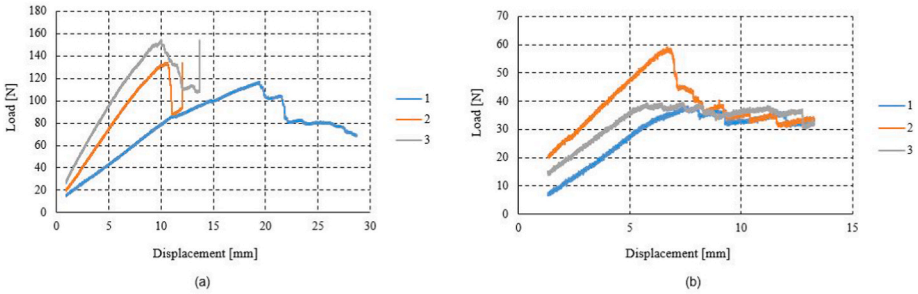

Fig. 12. Typical load-displacement curves of the (a) 3D and (b) 2D composites in the DCB test.

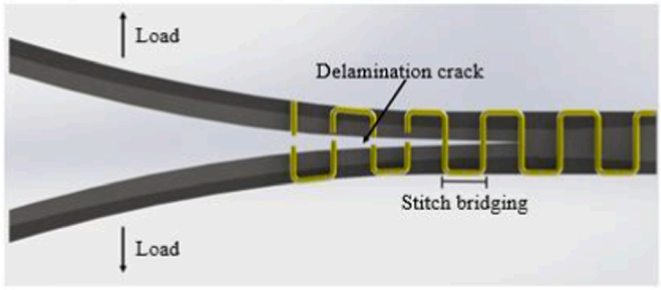

Fig. 13. Schematic drawing of delamination crack inhibited by stitch bridging.

Table 4
DCB test data.

Specimens	Maximum load [N]	Maximum displacement [mm]	Final length of delaminations crack [mm]	G_{Ic} [N/mm]
3D	135.18 ± 18.61	22.41 ± 5.58	1.03 ± 0.08[a]	–
2D	45.71 ± 11.73	14.13 ± 0.74	65.50 ± 24.96[b]	0.32 ± 0.05

[a] The measurement was taken from the microscopy images.
[b] The measurement was performed based on the calculation of the crack length value (Equation (4)).

3D counterparts, emphasizing the nearly complete inhibitory effect provided by the reinforcement tow. Both composites initially had identical crack lengths of 60 mm, with the final values presented in Table 4 excluding the initial length. It's crucial to clarify that the table value reflects the conclusive delamination length determined through optical microscopy. Specifically for 3D composites, a conventional graph correlating crack length with G_{Ic} would inaccurately represent the values. This is because the primary failure mechanism involves not only stable delamination propagation but also the bending of the sample arm. The table value serves the purpose of facilitating a qualitative comparative analysis, highlighting minimal crack propagation attributed to the presence of stitching.

Illustrated in Fig. 14, the propagation of the delamination crack within the midplane of a 3D composite specimen showcases well-developed stitch bridging zones, resulting in a 1.03 mm extension from the initial crack length. Additionally, it is evident that the delamination propagates without completely breaking the initial sewing thread, aligning with expectations. Furthermore, the presence of fiber bridges, as shown in Fig. 11, is observed. This might be associated with a delamination inhibition mechanism prevalent in FPR composites subjected to the DCB test. It is crucial to note that while fiber bridges are present in both 2D and 3D composites, they are less effective in preventing catastrophic failure in composites.

Despite the lack of determination of G_{Ic} for 3D composites, which

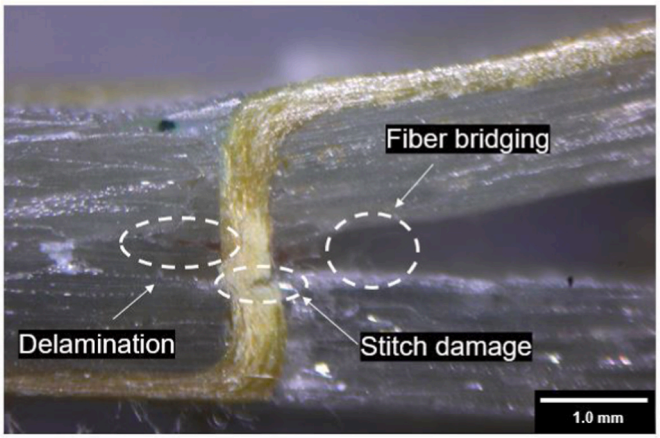

Fig. 14. Failure mechanisms present in 3D composite samples in the DCB test.

prevented a direct quantitative and comparative analysis with 2D laminates, the outcome of this test was anticipated. This anticipation arises from the fact that the literature largely presents data indicating an improvement in interlaminar fracture toughness caused by the stitching process [14,17–19].

In contrast to flexural properties, it is observed that high values of stitching density and reinforcement tow diameter have a positive influence on interlaminar fracture toughness, effectively impeding delamination crack propagation. However, it is evident that the isolated increase in this property does not guarantee the high applicability of these materials, as it may be associated with the simultaneous deterioration of other properties. Therefore, achieving a balance in stitching density and tow diameter values is crucial, aiming not only to increase G_{Ic} but also to optimize other essential properties according to project requirements.

Finally, there is a highlighted need for the development of new techniques to assess the interlaminar fracture toughness of stitched 3D composites. This is due to the fact that stitching can virtually prevent delamination propagation, leading composites to fail through other mechanisms.

3.5. Interlaminar shear strength

Fig. 15 presents the shear stress-displacement curve, revealing distinct phases in the mechanical behavior of both composites. Initially, a linear growth characterizes the elastic deformation regime of the materials. Subsequently, both composites transition into an inelastic regime preceding failure. This inelastic regime, attributed to matrix plastification and the presence of damage, is noteworthy. The divergence in interlaminar shear properties between the composites is most apparent in terms of maximum strength: 2D composites exhibit a strength of 48.92 ± 1.15 MPa, while 3D composites display a slightly lower strength of 39.71 ± 1.22 MPa.

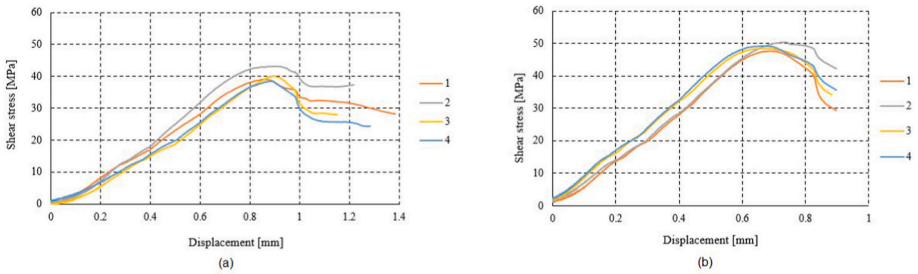

Fig. 15. Typical stress-displacement curves of the (a) 3D and (b) 2D composites in the SBS test.

Notably, even after global failure (post maximum load), 3D composites exhibit an increase in point load. This intriguing phenomenon is a result of sequential stitch line failure. As each stitch line gives way, the crack advances to the next, offering resistance against delamination and consequently leading to a punctual increase in load. This phenomenon observed consistently in the Three-points bending and DCB tests as well, significantly enhances the damage tolerance of 3D composites by averting sudden catastrophic failure.

The observed 18 % reduction in interlaminar shear strength in stitched 3D composites can be attributed to an analysis of the underlying failure mechanisms. In 2D composites, as the applied load increases, the primary failure mode involves delamination-induced cracking, which is accompanied by the development of matrix cracks and fiber rupture due to microbuckling. However, in 3D composites, even though the failure mode remains similar, the initiation of damage takes place at lower stress levels. These findings diverge from the common trend where several authors have reported significant improvements in interlaminar shear strength as a result of the impact of the stitching process on in-plane fibers [21,42,43]. However, a more thorough analysis of the influence of stitching on shear strength is necessary, especially because the stitching pattern seems to have a significant impact on this property. As reported by He et al. [20], if the damages caused by the stitching process are not within the loaded region, the negative effects they cause can be mitigated. This observation may even be extended to other tests, such as bending and impact, aiming to improve other properties as well. It is worth noting that the ability to reinforce only the desired region is one of the significant advantages of stitching compared to other 3D reinforcement techniques and should be further explored in the future.

The failure process in 3D composites can be segmented into two stages. Firstly, the initiation and propagation of delamination cracks in the midplane are strongly suppressed by the stitches, contrasting the behavior observed in 2D composites (Fig. 16a). Subsequently, as the load escalates, new modes of damage emerge in the material. These encompass debonding of reinforcing tows from the matrix (Fig. 16b) and fiber rupture due to microbuckling, resulting in the formation of kinking bands. Notably, unlike in 2D composite samples, kinking band regions in 3D composites do not give rise to delaminations around them (Fig. 17).

It is imperative to acknowledge that the short-beam interlaminar shear strength test deviates from a direct representation of pure shear, which would be ideal for a shear test. The complexity arises from the shear stress distribution along the specimen, which varies parabolically from zero at the top and bottom surfaces, to a maximum at the mid-plane. In contrast, bending stresses (tensile and compression) peak on the surfaces and decrease linearly to zero at the mid-plane. These stresses also exhibit a linear variation along the beam's length, ranging from zero at the supports to a maximum at the load point [44]. Consequently, while not an exact simulation of pure shear, this test yields reasonable interlaminar shear strength values, particularly for comparative analysis between materials.

In conclusion, akin to the comparative analysis of bending properties between 3D and 2D composites, the lower interlaminar shear strength of three-dimensionally reinforced composites is offset by their remarkable capacity to maintain structural integrity post-failure. Furthermore, the failure mode observed in this test parallels that witnessed in the Three-points bending test, albeit with the distinct addition of the reinforcement tow debonding mechanism.

4. Summary and conclusions

This study delved into a comprehensive comparative analysis of the mechanical characteristics of 3D stitched and 2D laminate composites, encompassing aspects such as bending, impact resistance, interlaminar fracture toughness, and interlaminar shear properties. Additionally, the investigation aimed to unravel the distinct failure modes exhibited by these two types of composites under varying loading conditions, shedding light on the outcomes of the experimental assessments. From the wealth of findings amassed, several key conclusions can be drawn.

- Within the realm of bending tests, a discernible trend emerged, showing that 3D composites encountered a reduction of 23 % in strength and 20 % in stiffness compared to their 2D counterparts. The beneficial influence of stitch bridging in curtailing the propagation of

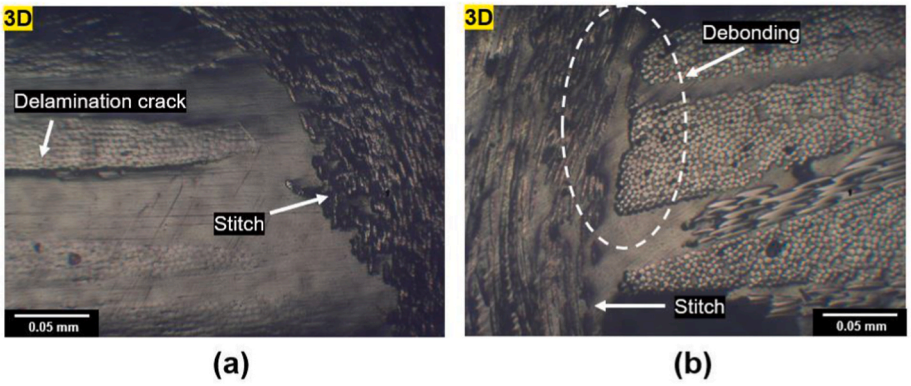

Fig. 16. Stitch-suppressed delamination crack and (b) Debonding of the reinforcing tow from the matrix.

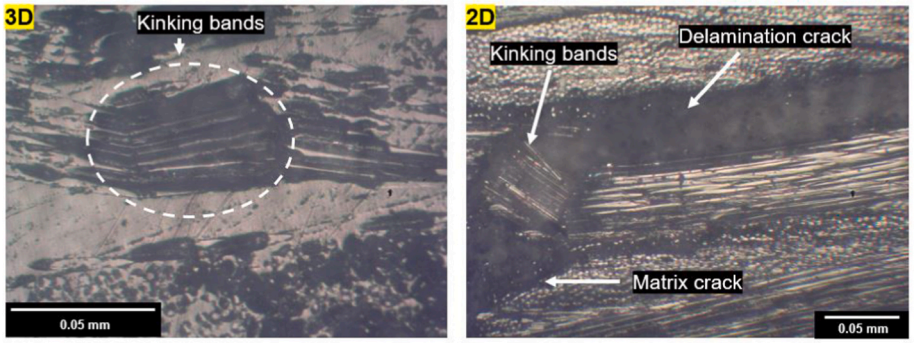

Fig. 17. (A) Fracture of fibers by microbuckling in 2D composite and (b) Fracture of fibers by microbuckling in 3D composite.

delamination cracks encountered counteraction from the detrimental effects induced by the stitching process itself. Factors such as fiber breakage, misalignment, crimping, and the emergence of resin-rich zones collectively contributed to the untimely failure of 3D composites.

- The response of impact toughness to low-energy impacts showcased limited responsiveness to stitching. Although the incorporation of reinforcement tows effectively suppressed the swift advancement of delamination cracks, a secondary outcome emerged in the form of shorter delaminations occurring in close proximity to the impact site.
- 3D composites exhibited an impressive interlaminar fracture toughness, even though quantifying the G_{Ic} value faced limitations due to the testing setup. The efficiency of the reinforcement tows in restraining delamination growth redirected the failure behavior towards alternate mechanisms, notably the bending of the sample arms.
- A noteworthy 19 % decrease in shear strength was observed in 3D composites, predominantly attributed to shear failures occurring at lower loads due to the structural damage introduced during the stitching process.

  Synthesizing insights from a spectrum of tests including three-points bending, Charpy impact, DCB, and SBS, it can be firmly asserted that 3D composites possess the capacity to uphold their structural integrity post-failure, due to the embedded reinforcement tows. Consequently, these composites exhibit an elevated level of damage tolerance when contrasted with their 2D counterparts.
- The intricate amalgamation of beneficial stitching effects, like the suppression of delamination cracks, with the associated drawbacks, encompassing fiber breakage, misalignment, crimping, and the creation of resin-rich regions, shapes the failure mechanism in 3D composites. This underscores the existence of optimal stitching parameters for each specific composite configuration, where the benefits strategically outweigh the drawbacks, leading to an overarching improvement in mechanical properties.

Declaration of competing interest

The authors declare that they have no known competing financial interests or personal relationships that could have appeared to influence the work reported in this paper.

Acknowledgments

The authors would like to express their gratitude to the Brazilian agency, CAPES, for research support, Texiglass® and Ephoxal® for supplying the necessary materials. They also extend their thanks to the Brazilian Laboratory of Composite Materials at IFSP-SC, the Laboratory of Aeronautic Structures (LEA) at USP-EESC, the Laboratory of Mechanical Properties (NEMAF) at USP-EESC, and the Laboratory of Metallography and Thermal Treatment at CEFET-RJ for providing the infrastructure.

References

[1] Xuan JQ, Li DS, Jiang L. Fabrication, properties and failure of 3D stitched carbon/epoxy composites with no stitching fibers damage. Compos Struct 2019;220:602–7. https://doi.org/10.1016/j.compstruct.2019.03.080.
[2] Song C, Fan W, Liu T, Wang S, Song W, Gao X. A review on three-dimensional stitched composites and their research perspectives. Compos Appl Sci Manuf 2022;153:106730. https://doi.org/10.1016/j.compositesa.2021.106730.
[3] Gnaba I, Legrand X, Wang P, Soulat D. Through-the-thickness reinforcement for composite structures: a review. J Ind Textil 2019;49(1):71–96. https://doi.org/10.1177/1528083718772299.
[4] Ma PS, Ye JY, Tian K, Chen XH, Zhang LW. Fracture phase field modeling of 3D stitched composite with optimized suture design. Comput Methods Appl Mech Eng 2022;392:114650. https://doi.org/10.1016/j.cma.2022.114650.
[5] Sela N, Ishai O. Interlaminar fracture toughness and toughening of laminated composite materials: a review. Composites 1989;20(5):423–35. https://doi.org/10.1016/0010-4361(89)90211-5.
[6] He Y, Mei M, Yu S, Wei K. Drop-weight impact behaviour of stitched composites: influence of stitching pattern and stitching space. Compos Appl Sci Manuf 2023;172:107612. https://doi.org/10.1016/j.compositesa.2023.107612.
[7] Prasad M, Sangeetha G, Rahul V, Anil Kumar A, Arulkumar R. Experimental study on flexural strength of stitched foam composites. Mater Today Proc 2023. https://doi.org/10.1016/j.matpr.2023.04.468.
[8] Song W, Liu T, Song C, Wang S, Jing Y, Ma J, et al. Effects of stitching yarn types on flexural fatigue properties of 3D stitched carbon fiber composites. Polym Test 2022;115:107744. https://doi.org/10.1016/j.polymertesting.2022.107744.
[9] Saboktakin A, Kalaoglu F, Shahrooz M, Spitas C, Farahat S. Failure analysis of 3D stitched composite using multi-scale approach for aerospace structures. J Textil Inst 2022;113(5):943–51. https://doi.org/10.1080/00405000.2021.1909800.
[10] Saboktakin A, Safaee H, Spitas C, Kalaoglu F. Stitched preform characterization for satellite structures. J Inst Eng Prod 2023;17(5):679–88. https://doi.org/10.1007/s11740-023-01187-6.
[11] Zhao N, Rödel H, Herzberg C, Gao SL, Krzywinski S. Stitched glass/PP composite. Part I: tensile and impact properties. Compos Appl Sci Manuf 2009;40(5):635–43. https://doi.org/10.1016/j.compositesa.2009.02.019.
[12] Ravandi M, Teo WS, Tran LQN, Yong MS, Tay TE. Low velocity impact performance of stitched flax/epoxy composite laminates. Composites Part B 2017;117:89–100. https://doi.org/10.1016/j.compositesb.2017.02.003.
[13] Kaya G, Soutis C, Potluri P. Flexural behaviour of unreinforced and Z-fibre reinforced 3D carbon/epoxy composites. Appl Compos Mater 2021. https://doi.org/10.1007/s10443-021-09949-0.
[14] Mouritz AP. Flexural properties of stitched GRP laminates. Compos Appl Sci Manuf 1996;27(7):525–30. https://doi.org/10.1016/1359-835X(96)00010-3.
[15] Mouritz AP, Gallagher J, Goodwin AA. Flexural strength and interlaminar shear strength of stitched GRP laminates following repeated impacts. Compos Sci Technol 1997;57(5):509–22. https://doi.org/10.1016/S0266-3538(96)00164-9.
[16] Nie J, Xu Y, Zhang L, Yin X, Cheng L, Ma J. Effect of stitch spacing on mechanical properties of carbon/silicon carbide composites. Compos Sci Technol 2008;68(12):2425–32. https://doi.org/10.1016/j.compscitech.2008.04.012.
[17] Velmurugan R, Solaimurugan S. Improvements in Mode I interlaminar fracture toughness and in-plane mechanical properties of stitched glass/polyester composites. Compos Sci Technol 2007;67(1):61–9. https://doi.org/10.1016/j.compscitech.2006.03.032.
[18] Dransfield KA, Jain LK, Mai YW. On the effects of stitching in CFRPs - I. Mode I delamination toughness. Compos Sci Technol 1998;58(6):815–27. https://doi.org/10.1016/S0266-3538(97)00229-7.
[19] Plain KP, Tong L. An experimental study on mode I and II fracture toughness of laminates stitched with a one-sided stitching technique. Compos Appl Sci Manuf 2011;42(2):203–10. https://doi.org/10.1016/j.compositesa.2010.11.006.

[20] He Y, Mei M, Wei K, Yang X, Duan S, Han X. Interlaminar shear behaviour and meso damage suppression mechanism of stitched composite under short beam shear using X-ray CT. Compos Sci Technol 2022;218:109189. https://doi.org/10.1016/j.compscitech.2021.109189.
[21] Mitschang P, Ogale A. Effect of sewing threads on interlaminar shear strength and flexural bending strength of stitched non-crimp carbon fabric laminates. Adv Compos Lett 2006;15(6):199–206. https://doi.org/10.1177/096369350601500602.
[22] Jain LK, Mai YW. Recent work on stitching of laminated composites – theoretical analysis and experiments. In: Elevated international conference on composite materials, organizer. Proceedings of the 11th ICCM congress; 1997. p. 25–51. July 14-18; Gold Cost, Australia.
[23] Liu T, Gao Y, Gao X, Yao Y, Lu Y, Fan W. A systematic investigation for mode-I fracture properties of stitched composites. Int J Mech Sci 2023;241:107982. https://doi.org/10.1016/j.ijmecsci.2022.107982.
[24] Song W, Fan W, Liu T, Chen X, Wang S, Zhao Y, et al. Flexural fatigue properties and failure propagation of 3D stitched composites under 3-point bending loading. Int J Fatig 2021;153:106507. https://doi.org/10.1016/j.ijfatigue.2021.106507.
[25] McDonnell C, Hayes S, Potluri P. Investigation into the tensile properties of ISO-401 double-thread chain-stitched glass-fiber composites. International Journal of Lightweight Materials and Manufacturing 2021;4(2):203–9. https://doi.org/10.1016/j.ijlmm.2020.11.001.
[26] Kim CH, Sim HW, An WJ, Kweon JH, Choi JH. Impact characteristics of composite panel stitched by I-fiber process. Compos Appl Sci Manuf 2019. https://doi.org/10.1016/j.compositesa.2019.105644.
[27] Zhang H, He R, Hou B, Li Y, Cui H, Yang W. Artificial hail ice impact damage of laminated composite T-joint with stitching reinforcement. Compos Struct 2021;278:114714. https://doi.org/10.1016/j.compstruct.2021.114714.
[28] Bilisik K, Karaduman NS, Sapanci E. Flexural characterization of 3D prepreg/stitched carbon/epoxy/multiwalled carbon nanotube preforms and composites. J Compos Mater 2019;53(5):563–77. https://doi.org/10.1177/0021998318787861.
[29] Alaziz R, Saha S, Sullivan RW, Tian Z. Influence of 3-D periodic stitching patterns on the strain distributions in polymer matrix composites. Compos Struct 2021;278:114690. https://doi.org/10.1016/j.compstruct.2021.114690.
[30] Gukendran R, Sambathkumar M, Raj TP, Nalinkumar S, Nivaas B, Kumar BSP. Effect of various stitching patterns on mechanical properties of jute fiber reinforced composite. Mater Today Proc 2023;80:882–7. https://doi.org/10.1016/j.matpr.2022.11.323.
[31] ASTM D7264/D7264M-07. Standard test method for flexural properties of polymer matrix composite materials. Annual Book of ASTM Standards; 2007. https://doi.org/10.1520/D7264.
[32] ASTM D6110-10. Standard Test method for determining the Charpy impact resistance of notched specimens of plastics. Annual Book of ASTM Standards; 2010. https://doi.org/10.1520/D6110-18.1.
[33] ASTM D5528-01. Standard test method for mode I interlaminar fracture toughness of unidirectional fiber-reinforced polymer matrix composites. Annual Book of ASTM Standards; 2014. https://doi.org/10.1520/D5528-13.2.
[34] ASTM D2344-00. Standard test method for short-beam strength of polymer matrix composite materials and their laminates. Annual Book of ASTM Standards; 2003. https://doi.org/10.1520/D2344_D2344M-22.
[35] Liu B, Lai J, Liu H, Huang Z, Liu B, Peng Z, et al. Experimental and numerical analysis of stitched composite laminates subjected to low-velocity edge-on impact and compression after edge-on impact. Polymers 2023;15(11). https://doi.org/10.3390/polym15112484.
[36] Tong L, Mouritz AP, Bannister MK. 3D fibre reinforced polymer composites. 1nd. ed. Amsterdam: Elsevier; 2002.
[37] Mouritz AP, Cox BN. A mechanistic approach to the properties of stitched laminates. Compos Appl Sci Manuf 2000;31(1):1–27. https://doi.org/10.1016/S1359-835X(99)00056-1.
[38] Mouritz AP, Cox BN. A mechanistic interpretation of the comparative in-plane mechanical properties of 3D woven, stitched and pinned composites. Compos Appl Sci Manuf 2010;41(6):709–28. https://doi.org/10.1016/j.compositesa.2010.02.001.
[39] Wood MDK, Sun X, Tong L, Katzos A, Rispler AR, Mai YW. The effect of stitch distribution on Mode I delamination toughness of stitched laminated composites - experimental results and FEA simulation. Compos Sci Technol 2007;67(6):1058–72. https://doi.org/10.1016/j.compscitech.2006.06.002.
[40] Hui C, Chen C, Legrand X, Wang P. Investigation of the interlaminar shear performance of tufted preforms and composites under mode II loading condition. Polymers 2022;14(4):1–13. https://doi.org/10.3390/polym14040690.
[41] Tanzawa Y, Watanabe N, Ishikawa T. FEM simulation of a modified DCB test for 3-D orthogonal interlocked fabric composites. Compos Sci Technol 2001;61(8):1097–107. https://doi.org/10.1016/S0266-3538(01)00003-3.
[42] Sun Y, Fan W, Song C, Gao X, Liu T, Song W, et al. Effects of stitch yarns on interlaminar shear behavior of three-dimensional stitched carbon fiber epoxy composites at room temperature and high temperature. Adv Compos Hybrid Mater 2022;5(3):1951–65. https://doi.org/10.1007/s42114-022-00526-y.
[43] Bilisik K, Karaduman N, Sapanci E. Short-beam shear of nanoprepreg/nanostitched three-dimensional carbon/epoxy multiwall carbon nanotube composites. J Compos Mater 2020;54(3):311–29. https://doi.org/10.1177/0021998319863472.
[44] Abali F, Pora A, Shivakumar K, Ghantae S. Modified short beam shear test for measurement of interlaminar shear strength of carbon-carbon composites. Apr. In: Structures, structural dynamics, and materials conference, organizer. Proceedings of the 41th AIAA congress; 2000. p. 3–6. https://doi.org/10.2514/6.2000-1480. Atlanta, USA.